High sensitive photonic crystal multiplexed biosensor array using H0 sandwiched cavities

Safia Arafa*, *Mohamed* Bouchemat, *Touraya* Bouchemat, and *Ahlem* Benmerkhi
Electronics Department, Université des frères Mentouri, Constantine 1, 25017 Algeria

Abstract. We theoretically investigate a high sensitive photonic crystal integrated biosensor array structure which is potentially used for label-free multiplexed sensing. The proposed device consists of an array of three sandwiched H0 cavities patterned above silicon on insulator (SOI) substrate; each cavity has been designed for different cavity spacing and different resonant wavelength. Results obtained by performing finite-difference time-domain (FDTD) simulations, indicate that the response of each detection unit shifts independently in terms of refractive index variations. The optimized design makes possible the combination of sensing as a function of location, as well as a function of time in the same platform. A refractive index sensitivity of 520nm/RIU and a quality factor over 10^4 are both achieved with an accompanied crosstalk of less than -26 dB. In addition, the device presents an improved detection limit (DL) of $1.24.10^{-6}$ RIU and a wide measurement range. These features make the designed device a promising element for performing label-free multiplexed detection in monolithic substrate for medical diagnostics and environmental monitoring.

1 Introduction

Label-free optical biosensors have recently attracted increasing interest for high-performance quantitative measurements without heterogeneity labeling provided by the fluorescent techniques. In particular, photonic crystal (PhC) biosensors, because of their strong capability to manipulate light propagation, their miniaturized size, their high spectral sensitivity and their minimal sample preparation, have generated substantial attention as an attractive candidate for available label-free systems [1–15]. The performance of these biosensors is evaluated by the ability to detect the small change of refractive index (RI). For resonant biosensors, this ability is expressed in terms of quality (Q) factor and sensitivity (S). The Q-factor is defined as $Q=\lambda_0/\Delta\lambda$, where λ_0 is resonance wavelength and $\Delta\lambda$ is the line-width of the resonance peak, It represents the strength of light confined in a cavity. The sensitivity of a device is reflected by the magnitude of light-matter interaction. Among all the different biosensor designs that have been developed, the biosensors based on PC coupled waveguide micro-cavities systems have attracted significant interests due to their compact size, high Q-factor and high S [10-15].

However, the design drawback of these biosensors is that they typically operate as point or single detection unit and the number of targets which can be screened for at once is relatively small. Recently, in order to overcome this drawback and to detect different analytes simultaneously on a single platform, sensor arrays using PhC have been developed. Examples of such systems include that of Mandal *et al*. [16] who have firstly proposed a nanoscale optofluidic sensor array based on 1D PhC silicon waveguide for label-free detection of biomolecular interactions in aqueous environments. Yang *et al*. [17] who have demonstrated a nanoscale PhC sensor array on monolithic substrates using a side-coupled resonant cavity. Olyaee *et al*. [18] have also demonstrated a sensor array based on side coupled H1 cavities to PhC waveguide where sensitivity of 165.45nm/RIU was obtained. In order to efficiently increase the integration density of sensor array and restrain the crosstalk between adjacent PhC sensors, Yang et al. [19] have reported the investigation of an integrated sensor array based on H0 cavities side coupled to parallel output waveguides with crosstalk value lower than -4dB. Further, Liu et al. [20] have proposed an optical PhC sensor based on a channel-drop configuration with a reflector and an additional PhC cavity. Simulation and experimental results showed a good agreement with RI sensitivity of 153nm/RIU. Recently, In order to reduce the crosstalk effect Huang *et al* [21] have proposed a label-free integrated ring-slot sensor array structure that exhibits a Q factor of 11.000 and a crosstalk value of less than -25.8 dB in water environment.

This work aims to investigate a high sensitive PhC integrated biosensor array structure, which is potentially used for label-free multiplexed sensing in aqueous environment. In order to further improve the detection level and simultaneously restrain the crosstalk value between the adjacent biosensors, the well-known technique of wavelength division multiplexing to

* Corresponding author: arafa.safia@gmail.com

spatially separate the integrated biosensor is used. Results obtained by performing FDTD simulations indicate that the response of each sensor unit to the RI variation is completely independent and the resonance spacing between the adjacent sensors is wide enough to ensure high multiplexed detection.

2 PHC sandwiched cavity design

In order to efficiently enhance the integration density of biosensor array and restrain crosstalk value between the adjacent detection units, the sandwiched cavity design is proposed where the operation of the proposed device as a biosensor is based on a cavity coupled waveguide system. The two waveguides are obtained by removing one row of air holes in the x direction. They are used to couple light in and out of the PhC cavity.

As shown in Fig. 1, the proposed structure consists of a hexagonal lattice of air holes (r=180.5 nm) patterned periodically with a lattice constant a (a=475 nm) on a silicon on insulator (SOI) slab with an effective index of n_{eff}=2.87 which corresponds to the effective index of the fundamental guided TE mode in a 230 nm thick silicon slab on silicon dioxide at the wavelength of 1550 nm. Perfectly matched layers (PML) conditions have been considered in the calculations to ensure no back reflection in the limit of the analyzed region [22].

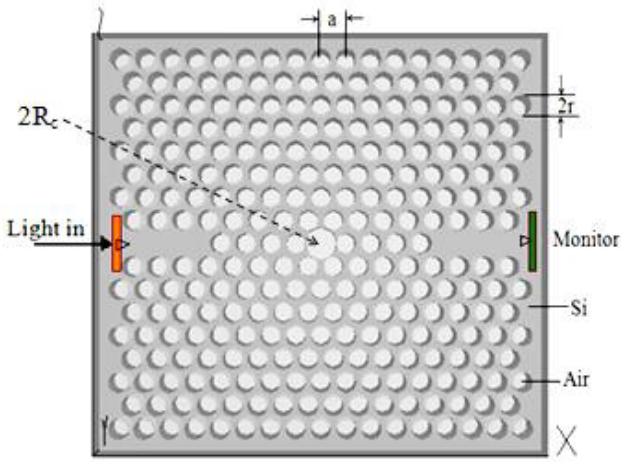

Fig. 1. Schematic diagram of the proposed PhC H0 cavity coupled to an input and output PhC waveguides. The resonator-waveguide system is patterned above a SO I substrate.

In the simulation process, a TE polarized Gaussian optical pulse, covering the whole frequency-range of interest, is launched at the input port to excite the cavity modes. A power monitor was placed at the end of the output waveguide to measure transmitted signal. For improving accuracy in the simulation, the 2D-FDTD analysis from the commercial RSoft software was carried out with a grid size of 0.01.

Obtained high RI sensitivity S ($\Delta\lambda/\Delta n$), which is defined as the ratio of the shift in the wavelength ($\Delta\lambda$) to the change in the RI due to analyte infiltration (Δn), depends largely on the increase of both the sensing surface and the Q factor value which increases the ability of the device to detect not only small concentrations, but also small changes in the analyte concentration. This can be achieved by increasing the radius of the central cavity hole (R_c).

The variation tendencies of the Q factor and the resonance wavelengths according to Rc change from 0.579a to 0.621a are plotted in Fig.2. According to the simulation results, we can note that, by increasing the radius of the central defect hole, the resonant peak shift to shorter wavelength (blue-shift) due to the decrease of the high-dielectric material in the cavity region. Similarly the Q factor gets promoted with the increase of R_c followed by a slight decrease and as seen in Fig.2 the air hole radius of Rc = 0.603a leads to an optimal design with a Q factor of 92963.

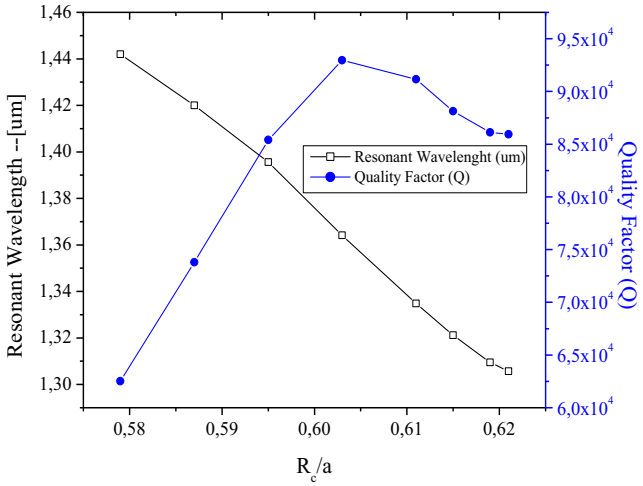

Fig. 2. The variation of the resonant wavelength and Q factor according to the change of the central hole radius.

It is essential to note that for biosensing applications, the magnitude of the resonant wavelength shift is dependent on the combination of many factors such as the number of functionalized holes and the effective refractive index change of targets.

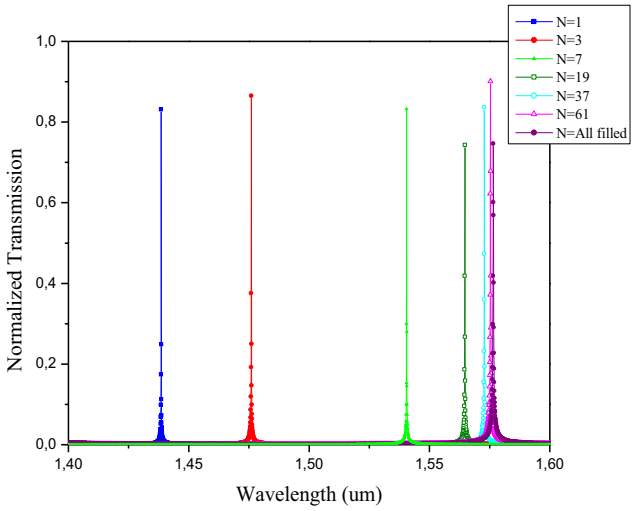

Fig. 3. Transmission spectra with different number of functionalized holes (N).

To study the dependence of the sensitivity on the number of functionalized holes, we varied the number of holes being functionalized (N) (filled with the analyte (DI-Water n=1.33) including the central defect hole and the surrounding holes around the resonant cavity.
The transmission spectra corresponding to the different infiltration cases (N varies from 1 hole being functionalized to the total filling of the PhC structure) are depicted in Fig.3. As can be seen in this figure, the resonant wavelength shift gets larger as the number of functionalized holes increases, which is due to the reduced effective refractive index between the infiltrated holes and the semiconductor membrane [23], as a result, the sensitivity becomes higher.

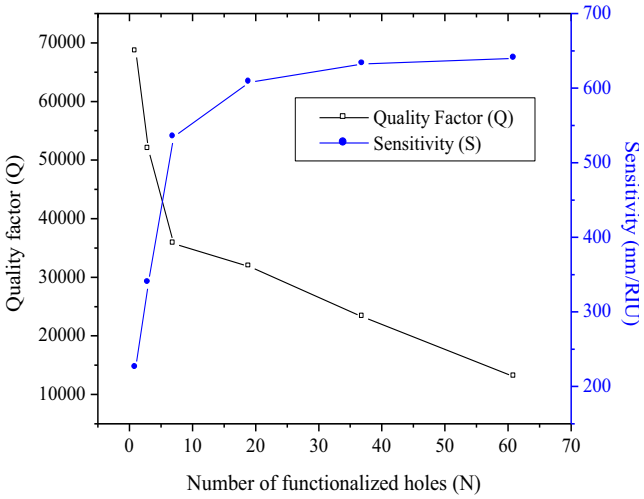

Fig. 4. Quality factor and refractive index sensitivity (S variations as a function of the number of functionalized circular holes (N).

The variation tendencies of the Q factor and sensitivity as a function of the change in the number o functionalized holes (N) that corresponds to the differen local infiltration cases are shown in Fig. 4.

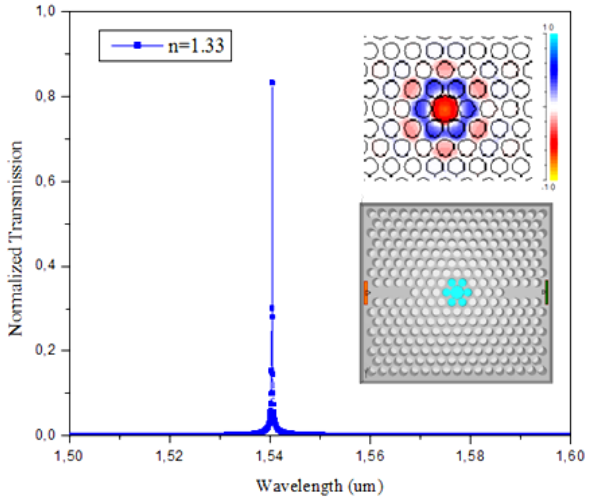

Fig. 5. The transmission spectra of the optimized PhC biosensor in water environment .the electric field distribution in x-y plane and the optimal structure design with the light blue functionalized area are represented in the inset figures.

As indicated in this figure, the sensitivity is enhanced by increasing the number of functionalized holes, whereas the Q factor is declined. Therefore, it has been necessary to choose a trade-off between the Q factor and the RI sensitivity. According to the obtained results, The optimal Q factor of 35718 and the improved sensitivity of 534.54 nm/RIU are both achieved for N=7 where the resonance peak is located at 1504.5 nm (Fig.5). These values present a large figure of merit compared to the finding of previous similar studies [13-15].
Further, we research the detection limit of refractive index, which is an important parameter in sensing applications. The detection limit of refractive index changes (DL) is expressed as follows [24]:

$$DL = \frac{\lambda_0}{10QS} \quad (1)$$

Where λ_0 represents the resonant wavelength, which is equal to 1504.5 nm, S is the RI sensitivity and Q means the quality factor. Based on the above results the calculated detection limit of the proposed biosensor is about 7.88×10^{-6} RIU.

3 PhC biosensors array design

Based on the design and discussion about the use of the sandwiched cavity as a RI biosensor in the above section, we demonstrate a PhC biosensor array with different three cavity spacing's and different resonant wavelengths integrated into a multiplexed array structure.

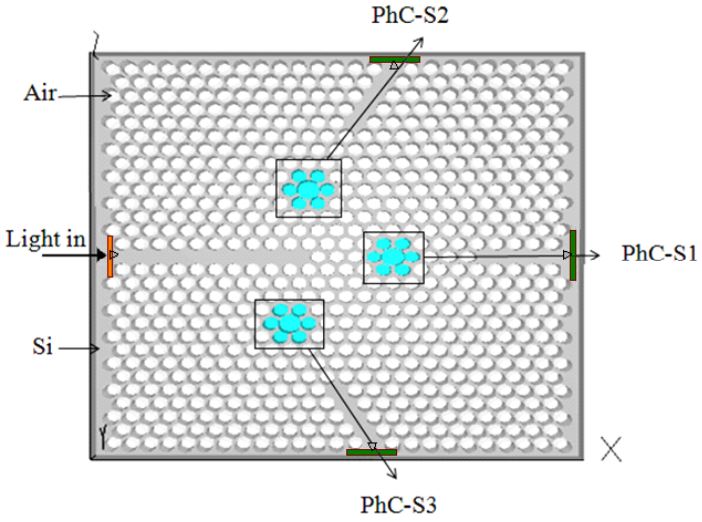

Fig. 6. Schematic diagram of the proposed PhC integrated biosensor array based on H0 sandwiched cavities. The light blue holes indicate the sensing area of each detection unit.

As shown in Fig.6, the specific parameters of the PhC biosensor array are set as follows: PhC-S1: R_{c1}=285; PhC-S2: R_{c2}=291, 5 nm; PhC-S3: R_{c3}=278, 5 nm. As it can be seen in Fig.7, the transmission efficiencies have response peaks at 1517.3 nm, 1547.2 nm and 1575.3 nm in water environment (RI = 1.33) with respect to the green, blue and red solid lines. It can also be noted that the three resonant wavelengths lie in the telecommunication wavelength region with an

appropriate resonant spacing and as expected they exhibit high transmission efficiency.

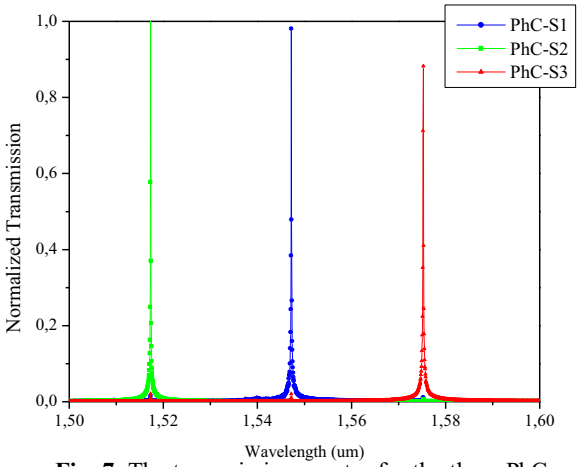

Fig. 7. The transmission spectra for the three PhC sandwiched cavities in water environment (RI=1.33).

The steady-state electric field profile for the fundamental TE-like mode propagation through the three cavities is shown in Fig.8. It can be clearly seen that the light is strongly confined within each resonant cavity, which means that the photon lifetime is enhanced and therefore higher Q factors can be achieved. The calculated Q factors of the three peaks are equal to 44360, 28710 and 25029 respectively. These values showed an improvement in respect to other reports [17-19, 21].

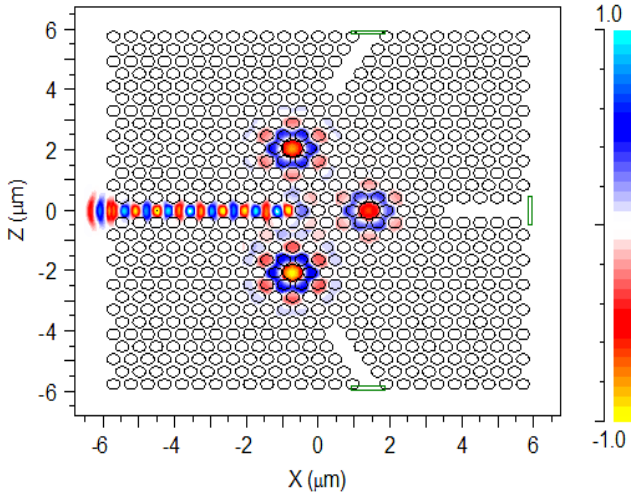

Fig. 8. Electric field distribution for the fundamental TE-like mode propagation, through the three cavities.

3.1. Sensing properties analysis of the integrated PhC biosensors array

To analyze the RI sensitivity of the PhC integrated sensor array in aqueous environment, the RI of the functionalized area of three biosensors is changed, respectively. Fig.9 shows the composed transmission spectra of the three sandwiched cavities (PhC S1, PhC S2, PhC S3) when the functionalized area of one biosensor is under RI changes and the others aren't.
As it can be seen from this figure, the shift occurs only with the functionalized biosensors while the others remain completely unchanged. It can also be noted that the spectral position of the resonating peak detected at the end of output waveguides shifts towards longer wavelengths (red-shift) as the RI of the biosensor functionalized area is increased by 1.330, 1.335, 1.340, 1.345, 1.350, 1.355, 1.360, 1.365, 1.370, 1.377, respectively, which is in good agreement with the previous works [21], [25].

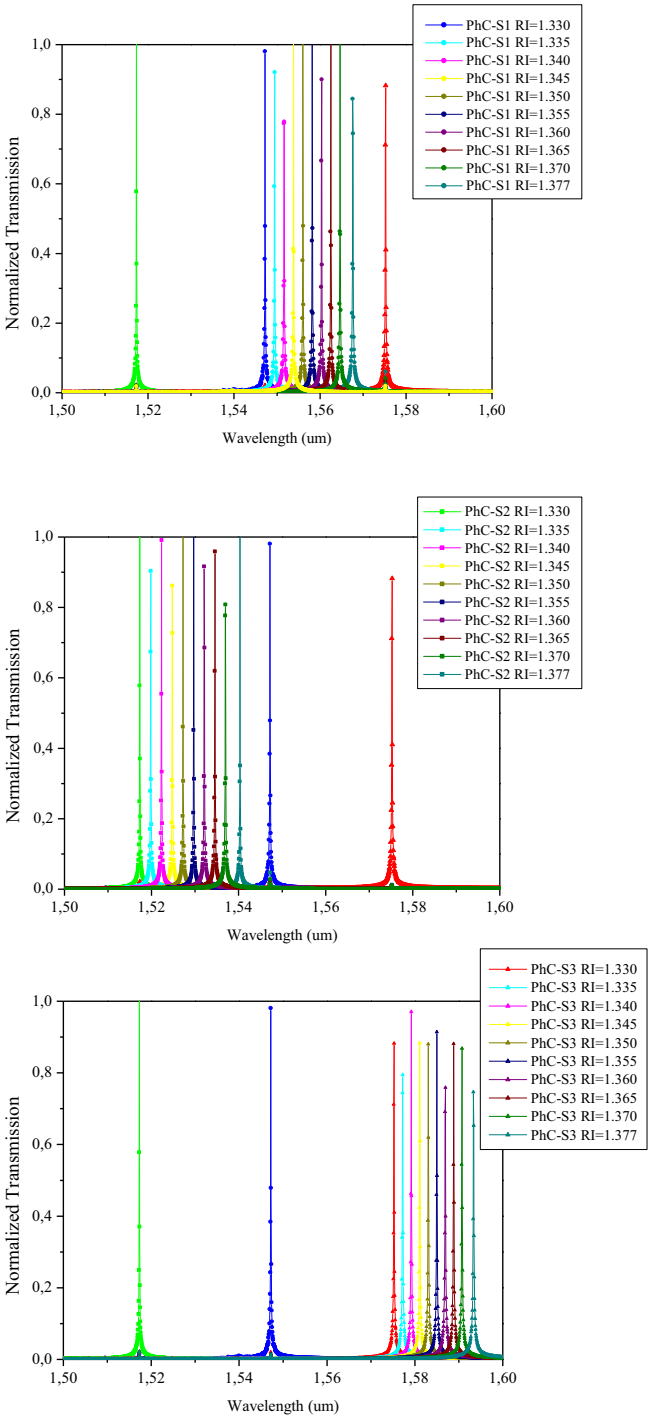

Fig. 9. The transmission spectra of the three sandwiched cavities (PhC S1, PhC S2, PhC S3) when the functionalized area of one sensor is under refractive index variations and the others are not.

Fig. 10 shows the resonance shift of each detection unit as a function of the RI variations. The colored shapes indicate the resonant wavelength shift values (Δλ) as a function of the RI variations (Δn), obtained from FDTD simulations and the red solid line is a linear fit. According to these results, the calculated RI sensitivities (S=Δλ/Δn) of the three biosensors are S1=440 nm/RIU, S2=520 nm/RIU and S3=400 nm/RIU, respectively. Based on Equation (1) the calculated detection limit of the proposed biosensor array is about 6.58x 10-6 RIU. These results are favorably comparable to the similar reported works [19, 21].

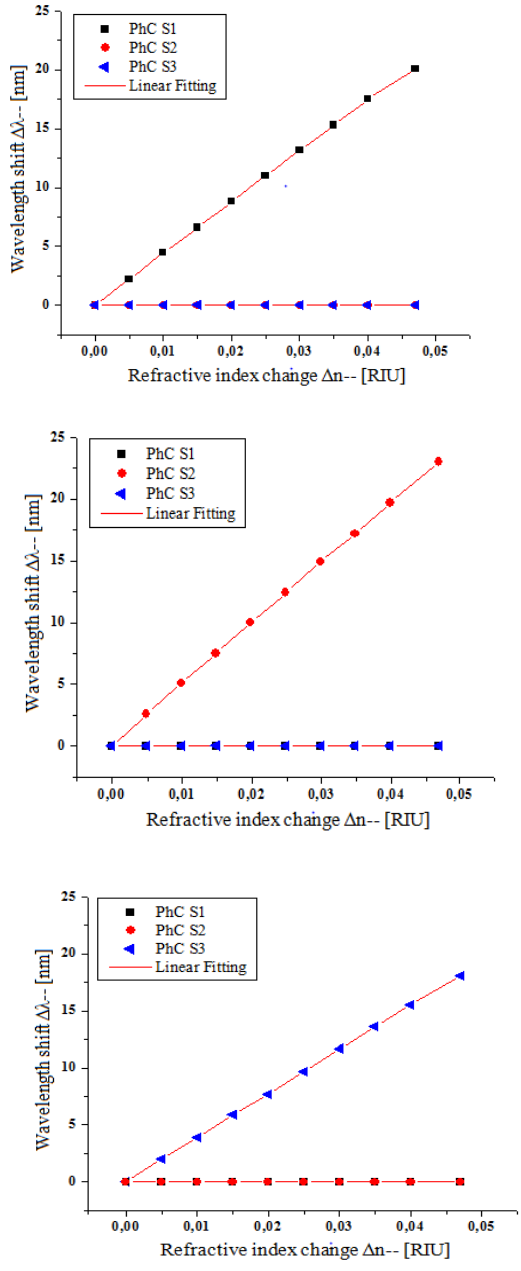

Fig. 10. Red shift in the resonant wavelength Δλ , as a function of the RI increases in the functionalized area and its associated linear fits (solid red line)

3.2 Crosstalk analysis of the integrated PhC biosensors array

The crosstalk between each biosensor unit is an important index for evaluating the component performances.
In this section, the crosstalk between each other adjacent detection unit is analyzed by performing a detailed simulation and by calculating the extinction ratio (ER) which is defined by the following equation: [21]

$$ER = 10\,log\,\frac{T}{T_i} \qquad (2)$$

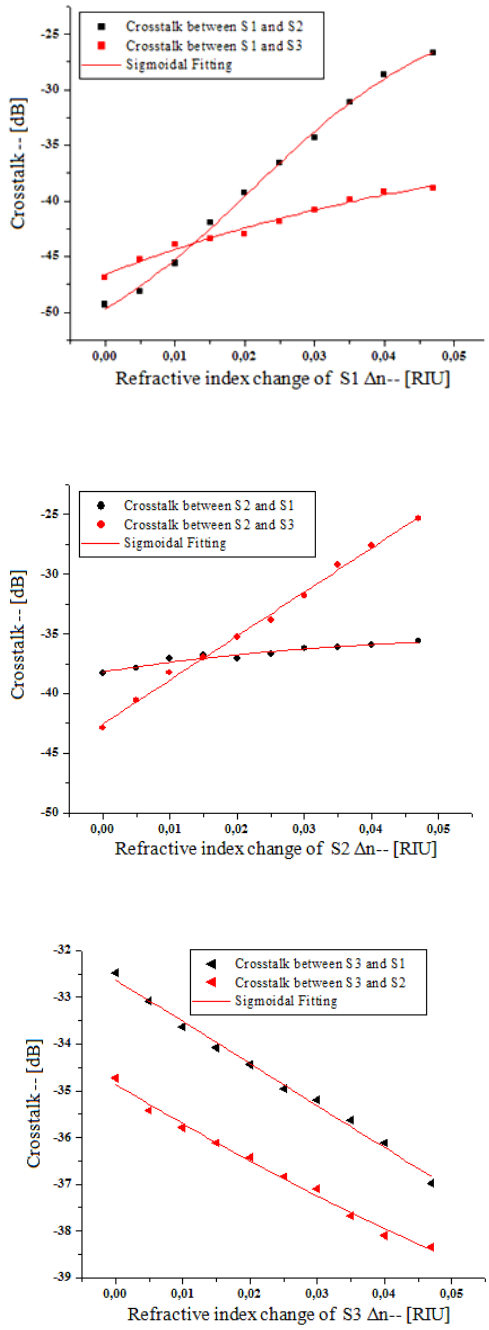

Fig. 11. The crosstalk (dB) between each other adjacent biosensor unit in the proposed biosensor array, when (a) PhC-S1, (b) PhC-S2, and (c) PhC-S3 is under the refractive index variations, respectively and the other biosensors are not.

Where:
T: The maximum transmission efficiency of one sensor at the resonant frequency ω_0 when the RI sensing area of this sensor is varied;
Ti: The minimum transmission efficiency of other adjacent sensors at the same the resonant frequency;
The calculated crosstalk between each other adjacent biosensors (PhC-S1, PhC-S2 and PhC-S3) in the proposed structure is shown in Fig. 10. The crosstalk is calculated when one sensor is exposed to RI variations and the others are not. As seen in this figure the crosstalk between each other adjacent sensor unit in the proposed PhC biosensor array lower than -26dB is observed.
The mean crosstalk value for the three sensors has been estimated to be lower than −26.12 dB. The obtained value has shown a great improvement compared to recent reported works [19, 26]. Furthermore, this value is in a good agreement with the results shown in [21], where the structural design proposed in this study is less complex. This low crosstalk value could potentially be very useful for monolithically integrated and multiplexed sensing technology.

4 Conclusion

In summary, a high sensitive PhC multiplexed biosensor array for label free biodetection has been reported and theoretically demonstrated. The parameters of each biosensor unit have been determined by adjusting the diameter of the central cavity hole, so that, the spectral response of each detection unit appears in telecom range. Simulation results indicated that the response of each biosensor to the RI variations was completely independent and the resonance spacing's between the adjacent ones were wide enough to ensure high parallel detection with an extremely low crosstalk value of -26.3 dB. Considering water absorption at telecom wavelength range, a RI sensitivity of 530 nm/RIU and a Q factor of 44360 have been both achieved with a detection limit of less than 6.57×10^{-6} RIU. The specific results suggest that the proposed device is a promising candidate for performing label-free multiplexed detection in monolithic platform.

References

1. E. Chow, A. Grot, L.W. Mirkarimi, M. Sigalas, G. Girolami, Opt. Lett, **29,** 1093-1095 (2004).
2. Y. Zhang, Y. Zhao, Q. Wang, Sens. Actuators B Chem, **209**, 431–437, (2015).
3. A. Benmerkhi, M. Bouchemat, T. Bouchemat, Optik, **127**, 5682–5687 (2016).
4. A. Benmerkhi, M. Bouchemat, T. Bouchemat, Photon. Nanostr. Fundam. Appl, **20**, 7-17, (2016).
5. N. Skivesen, A. Tetu, M. Kristensen, J. Kjems, L.H. Frandsen, P.I. Borel, Opt. Express, **15**, 3169-3176, (2007).
6. H.S. Dutta, S. Pal, Opt. Quantum Electron, **45**, 907–917, (2013).
7. H.S. Dutta, A.K. Goyal, S. Pal, J.Nanophotonics, **8**, 083088–083088, (2014).
8. F. Bougriou, T. Bouchemat, M. Bouchemat, N. Paraire, Eur. Phys. J. Appl. Phys, **62**, 11201-11206, (2013).
9. Y. Zhang, Y. Zhao, Q. Wang, Sens. Actuators B Chem, **184**, 179–188, (2013).
10. X. Wang, Z. Xu, N. Lu, J.Zhu, G. Jin, Opt. Commun, **281**, 1725–1731, (2008).
11. L. Huang, H. Tian, D. Yang, J. Zhou, Q. Liu, P. Zhang, Y. Ji, Opt. Commun,**332**,42-49,(2014).
12. S. Arafa, M. Bouchemat, T. Bouchemat, A. Benmerkhi, A. Hocini, Opt. Commun, **384**, 93-100, (2017).
13. A. Harhouz, A. Hocini, J. Electromagn. Wave Appl, **29**,659–667, (2015).
14. J. Zhou, H. Tian, D. Yang, Q. Liu, Y. Ji, Opt. Commun, **330**, 175–183, (2014).
15. L. Huang, H. Tian, J. Zhou, Q. Liu, P. Zhang, Y. Ji, Opt. Commun, **335**, 73–77, (2015).
16. S. Mandal, D.Erickson, Opt. Express, **16**, 1623–1631, (2008).
17. D. Yang, H. Tian, Y. Ji, Opt. Express, **19**, 20023–20034, (2011).
18. S. Olyaee, S. Najafgholinezhad, Appl. Optics, **52**, 7206-7213, (2013).
19. D. Yang, H. Tian, Y. Ji, IEEE Photonics J, **6**, 1–7 (2014).
20. Y. Liu, H.W.M. Salemink, J. Lightwave Technol, **33**, 3672–3678, (2015).
21. L. Huang, H. Tian, J. Zhou, Y. Ji, Sensors, **14**, 15658–15668 (2014).
22. J. P. BerengerJ. Comput. Phys.**114**, 185–200 (1994).
23. A. Faraon, D. Englund, I. Fushman, J. Vučković, N. Stolz, P. Petroff Appl. Phys. Lett. **90**, 213110–213113, (2007).
24. I.M. White, X. Fan, Opt. Express, **16**, 1020–1028, (2008).
25. S. Arafa, M.Bouchemat, T. Bouchemat, A. Benmerkhi, Optik, **131**, 49-57, (2017).
26. P. Zhang, H. Tian, D. Yang, Q. Liu, J. Zhou, L. Huang, Y. Ji, Opt. Commun, **355**, 331–336, (2015).